Open form pressure balancing for compliant hydrostatic thrust bearings

Nijssen, Joep; van Ostayen, Ron

DOI
10.1007/978-3-030-20131-9_395

Publication date
2019

Document Version
Final published version

Published in
Advances in Mechanisms and Machine Science

Open Form Pressure Balancing for Compliant Hydrostatic Thrust Bearings

Joep Nijssen[1] and Ron van Ostayen[1]

Delft University of Technology, Section of Precision and Microsystem Engineering, Mekelweg 2, 2628CD Delft, The Netherlands,
J.P.A.Nijssen@tudelft.nl

Abstract. Traditionally hydrostatic slider bearings have rigid surfaces, and therefore require a well-defined and rigid counter surface with a constant or zero curvature. However, when the counter surface has a curvature varying along the path of the hydrostatic bearing, that hydrostatic bearing needs to follow that curvature. For this bearing compliance is required. This work introduces a new principle to increase the performance of compliant hydrostatic bearings by means of open form pressure balancing. A numerical example is provided to show the potential by comparing axi-symmetric parallel bearing performance of different geometries. Using thin-film assumption, the model is solved using an elasto-hydrostatic approach. The film height, pressure profile and load capacity are presented. This work provides the initial findings for pressure balanced parallel bearings.

Keywords: Static balancing, pressure balancing, hydrostatic thrust bearings, externally pressurized bearings, elasto-hydrostatic, compliant bearings

1 Introduction

Hydrostatic thrust bearings are machine components highly suitable for reliable motion performance because of their high load capacity, very low friction and minimal wear. The formation of the lubricating film is key in successful operation. Classic hydrostatic thrust bearings consist of rigid components, and this creates the need for smooth and rigid counter sliding surfaces. Especially for large machines and large sliding surfaces, this is a costly investment. This also limits the use of hydrostatic bearings to linear or constant curvature guiding systems. Flexible or compliant hydrostatic bearings allow for a far less critical slide surface, and rubber supported hydrostatic bearings have been investigated previously [1], [2], [3]. However, these bearings have fundamental limitations. The relation between the amount of surface irregularity the bearing allows for at a given design load can be defined by its bending stiffness k_B. The relation between the compression of the bearing and this load condition can be defined by its compression stiffness k_C. A visual representation is seen in figure 1. This ratio between these types of stiffness is defined in this work as $\zeta_k = k_C/k_B$. Simply by

T. Uhl (ed.), *Advances in Mechanism and Machine Science*,
Mechanisms and Machine Science 73,
https://doi.org/10.1007/978-3-030-20131-9_395

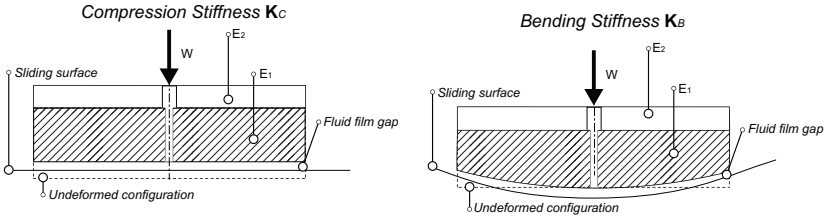

Fig. 1. Both stiffness definitions, with the undeformed configuration being the original unloaded bearing geometry.

changing material from metal to rubber like has been done in [1], [2], [3] does decrease the stiffness magnitude of both k_{C} and k_{B}. The ratio however remains unchanged. Either the bearing has high stiffness and therefor high load capacity, or low stiffness and therefor high deformability. in both cases the stresses are limiting the bearing performance.
To break this paradigm of exchanging load capacity for deformability, different approaches can be made. One would be to change the stiffness ratio ζ_{k} by ways of innovative bearing geometry design. This would require designing geometries that have a high k_{C} and a low k_{B} and therefor having a high stiffness ratio. Another approach would be to create a very low stiffness bearing, where k_{C} and k_{B} are both low, while maintaining the overall load capacity of a high k_{C} bearing. This work explores the second option by ways of open form pressure balancing. The principle will be explained and a simple, design example is used to show its potential. The open form pressure balanced design will be compared with solid and non-balanced counterparts.

2 Methods

Pressure balancing can be seen a fluid pressure induced version of static balancing [4]. By using the pressurized operation fluid used in the bearing to internally pressurize the bearing, higher load capacities can be achieved without stress limitations. Static balancing is used in a variety of mechanisms to achieve loaded flexible systems. Since a pressurized operation fluid is present in hydrostatic bearing, it can be used as a source of balancing force. The use of closed form fluid chambers has been used in dampers [5] to remove energy from a moving system. The method presented here relies on open form pressure balancing, where the volume of the fluid can change, by connecting the pressure chambers to the fluid film. This causes the fluid volume in the chambers to be variable. By having an open fluid volume, its internal pressure is shape indepenent. A basic pressure balanced bearing geometry can be seen in figure 2. If $E_1 \ll E_2$ then just having such a geometry without internal pressure would have a low compression and bending stiffness and a low load capacity because stresses will be limiting.

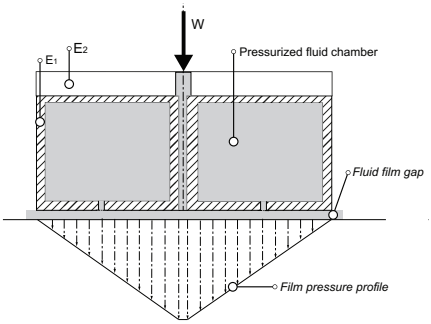

Fig. 2. Cross section of a parallel thrust bearing with pressure balancing chambers. The chambers are connected to the pressure film, having equal pressure to the pressure at that location of the profile.

By using pressure balancing, the load capacity can increase since the bearing becomes statically balanced, but the stiffness remains low, since the stiffness of the geometry is low and the chambers do not add stiffness. Having low stiffness allows for greater deformability. This principle could potentially allow for the design of a highly compliant bearing with a load capacity comparable to its high stiffness counterparts.

2.1 Computational model

To present a number of effects pressure balancing has on bearing performance, a computational model is used. The three axi-symmetric geometries seen in figure 3 will be compared to each other. One of the most basic bearing geometries is

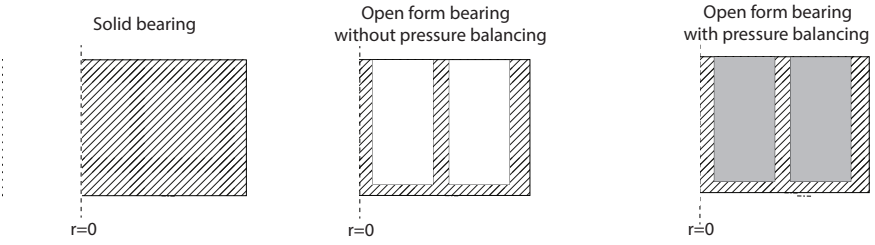

Fig. 3. Three geometries that will be compared.

circular with zero recess and a linear restrictor. This basic bearing geometry will be used for all 3 cases to present the principle. The hydrostatic film pressure and stress within the bearing becomes dependant on the elastic deformation of the bearing surface, making it an elasto-hydrostatic problem. The material is

modelled using a linear elastic material model. The bearing will be modelled as a 2D axi-symmetric model using Comsol Multiphysics. It's open form geometry, which has equal radius and height to the solid bearing, can be seen in figure 4. The hydrostatic problem is modelled using the axi-symmetric form of the

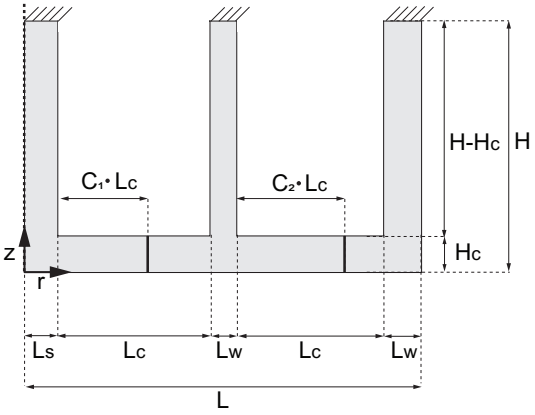

Fig. 4. Lay-out of computational model that will be used to analyse potential of pressure balancing.

Reynolds' equation [3].

$$\frac{\partial}{\partial r}(-\frac{h_{\mathrm{e}}^3 r}{12\eta}\frac{\partial p_r}{\partial r}) = 0 \tag{1}$$

To take into account the effects of elasto-hydrostaticity, the film thickness h_{e} is described as:

$$h_{\mathrm{e}} = h_0 + w \tag{2}$$

Where h_0 is the initial film thickness and w is the elastic deformation of the bearing at the boundary $z = 0$, $r \in [0 : L]$ caused by the pressure profile described by the Reynolds' equation. Lastly, $h_{\min}$ is an absolute minimum value of the film height used to prevent convergence issues due to the deformation causing a zero or negative film height. The load capacity F_p of the bearing is found by integrating the pressure P_r over this circular boundary. The model makes use of a Linear restrictor described as:

$$Q_{\mathrm{s}} = \frac{P_{\mathrm{s}} - P}{L_{\mathrm{r}}} \cdot \frac{\pi d_r^4}{128\eta} \tag{3}$$

Where L_r is the restrictor length, d is the restrictor diameter and η is the dynamic viscosity. Since the open form method couples the chamber pressure to a pressure location in the film, the variables C_1 and C_2 are introduced. Both variables range from 0 to 1, where 0 is the left corner of the chamber and 1 the

right corner. The pressure value at the location $z = 0$, $r = L_s + C_{1,2} \cdot L_c$ will determine the pressure in the left and right chamber respectively. A visualisation of the pressure balancing of the chambers can be seen in figure 5.

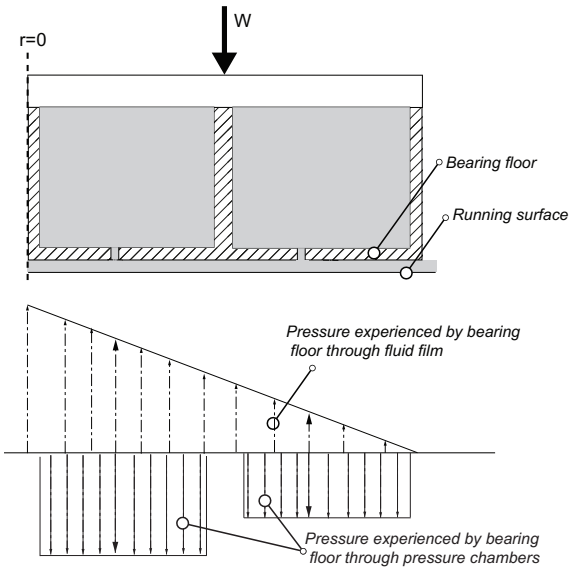

Fig. 5. Vizualization of how the chambers are connected to the fluid film and therefor have equal pressure compared to that specific location.

2.2 Modelling of surface irregularity

Initially the performance of pressure balancing will be compared to its solid competitors by using a flat sliding surface. However, as stated before, the interest of these bearings is in its capabilities to function under surface irregularities. To compare performance, convex and concave slide surfaces can be introduced. This counter surface is modelled as an additional film height h_c as:

$$h_c = A_c \cdot (\frac{r}{L})^2 \tag{4}$$

Where A_c is the maximum depth of curvature expressed in micrometres. Subtracting from the film thickness h_e will result in a concave surface, adding results in a convex one as illustrated in figure 6.

2.3 Case study

The focus on this work in terms of performance is based on the following characteristics:

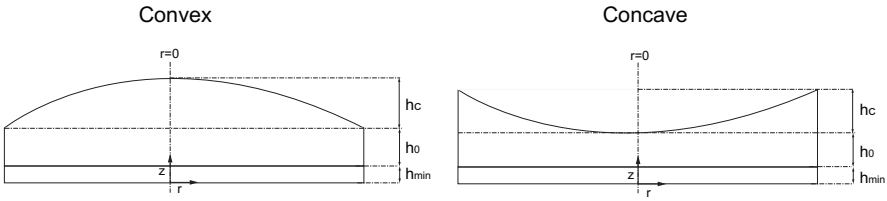

Fig. 6. Modelling of surface irregularity through convex and concave slide surfaces. Here h_c defines the curvature, h_0 the initial film and h_{min} the minimal film thickness to prevent instability in the numerical model.

1. Bearing load-displacement
2. Deformability

The objective is to use pressure balancing to create a bearing with comparable performance to a high stiffness solid bearing, which is for a parallel bearing defined as creating a parallel bearing surface to the slide surface. The film height is defined by the bearing surface lowest point over length L. A case study is performed to analyse the effects on performance caused by open form pressure balancing. The case study makes use of the geometry defined in figure 4. The dimensions used for the case study can be seen in table 1. As for the material, the Youngs Modulus equals that of rubber assuming the small strain approximation.

Table 1. Case study parameter values.

Parameter	**Value (unit)**
L	0.026 m
H	0.01 m
L_c	0.01 m
L_s	$L_c/10$
L_w	$L_c/4$
H_c	$L_c/5$
L_r	$L_c/10$
d_r	$L_c/100$
E	0.01 GPa
P_s	$E/100$

3 Results

To compare the pressure balanced geometry with its solid counterpart, the load-displacement performance of solid geometries is first analysed. A stiff material bearing ($E = 200$ GPa) is first compared with a rubber bearing ($E = 0.01$ GPa).

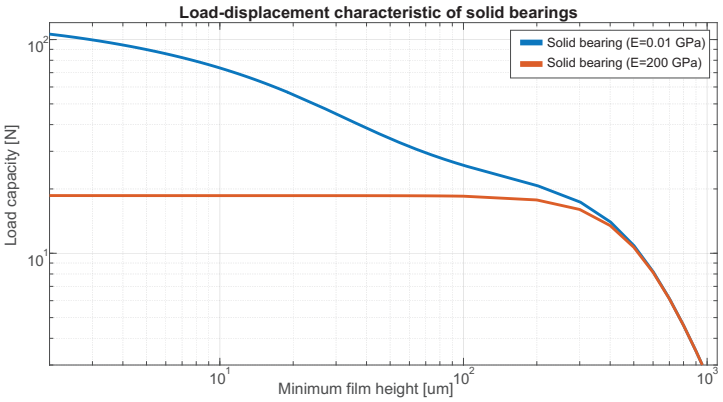

Fig. 7. Load-displacement of the solid geometry with different values for E. Here the effects of elasto-hydrostatics become visible through the difference of the two bearings.

The bearings are analysed with a counter surface having zero curvature, meaning $h_c = 0$. The resulting force-displacement can be seen in figure 7. The elasto-hydrostatic effects are clearly visible, where the solid rubber bearing creates a virtual recess through elastic deformation, resulting in a higher load capacity. The limitation of the rubber bearing however can be seen by looking at the peak stress values. This expressed in the following stress ratio:

$$\lambda_{\text{stress}} = \frac{E}{\sigma_{\text{mises}}} \tag{5}$$

Where σ_{mises} is the highest occuring Von Mises stress value. For the rubber bearing this results in a $\lambda_{\text{stress}} = 125$, while for the stiff bearing this results in $\lambda_{\text{stress}} = 5.7 \cdot 10^7$. A high stress factor λ_{stress} is equal to higher bearing lifetime. This stress factor is the last performance criteria used when analysing the effects of pressure balancing. The effects of chamber supply locations C_1 and C_2 are also investigated. This is done by choosing a fixed operational value of $h_0 = 10$ μm as well as having a curvature $h_c = 0$ over the entire bearing length. Resulting load capacity for different values of C_1 and C_2 at this operational film height can be seen in figure 8. Both C_1 and C_2 are only plotted from 0.5 since smaller values create numerical instability throughout convergence. A lower value of $C_{1,2}$ corresponds to a higher pressure value for a no recess bearing on a flat slide surface as seen in figure 5. The general trend of the desired pressure in the chambers is the higher chamber pressures creates a more parallel bearing

3.1 Load-displacement and pressure profiles

The Load-displacement of the different bearings configurations presented in figure 3 can be seen in figure 9, where a flat sliding surface ($h_c = 0$) is used. By

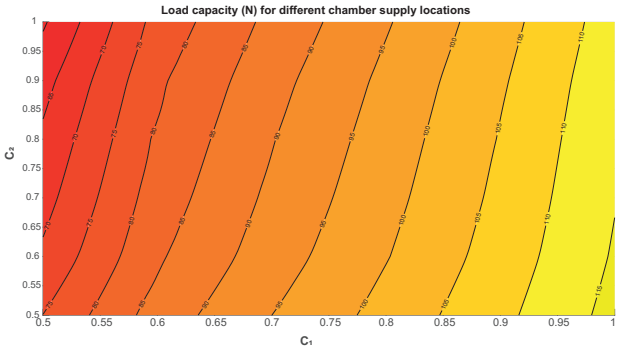

Fig. 8. Effects of changing chamber connection point on the load capacity. The lower load capacity is an indication of a more parallel bearing, meaning a low value of both C_1 and C_2 is desired. The optimum however is when C_1 has a low value while $C_2 = 1$ giving the lowest load capacity and therefor the most parallel bearing. The contour lines respresent the load capacity for different values of C_1 and C_2.

finding the minimum value over the boundary $z = 0$, $r \in [0 : L]$ and determining the load capacity, the Load-displacement performance can be determined. For displacement steps of h_0 defined as $X \leq S \leq X$, stepsize $S = 100$ μm was used between range 100 μm $\leq S \leq$ 1000 μm, stepsize $S = 10$ μm between 10 μm $\leq S \leq 100$ μm and stepsize $S = 1$ μm between -10 μm $\leq S \leq 10$ μm. h_0 can be negative because of elasticity of the bearing still causing the total film height h_c to be positive. A maximum value statement is used in Comsol MultiPhysics when defining h_e to make prevent negative film heights, by always having the lowest value of $h_e = h_{min} = 1$ μm. It was found that $C_{1,2} = 0.5$ could achieve the highest chamber pressure with numerical stability. The final pressure profiles of all configurations at lowest film height (2 μm) can be seen in figure 10. The ratio λ_{stress} for the open geometry and open geometry with pressure balancing are $\lambda_{stress} = 9.5$ and $\lambda_{stress} = 103$ respectively. Here the significance in stress levels can be seen, with the pressure balanced version having a significantly lower stress factor. The increasing load capacity of the non-balanced open geometry might seem favorable, but comes at the cost of high stresses.

3.2 Effects of curvature

In this work only the effect of adding a convex slide surface is analysed. The effects of contact are not taken into account, but all analyzed geometries show some form of contact (in this model meaning $h_c = 1$ μm) at the edges when analysing the effects of curvature. The entire model is still analysed using the film film Reynolds' approximation. By adding the constraint that 2 % of the bearing length is allowed to be in contact (meaning $h_c = 1$ μm), all elastic configurations can be compared. All elastic configurations are analysed by increasing A_c untill

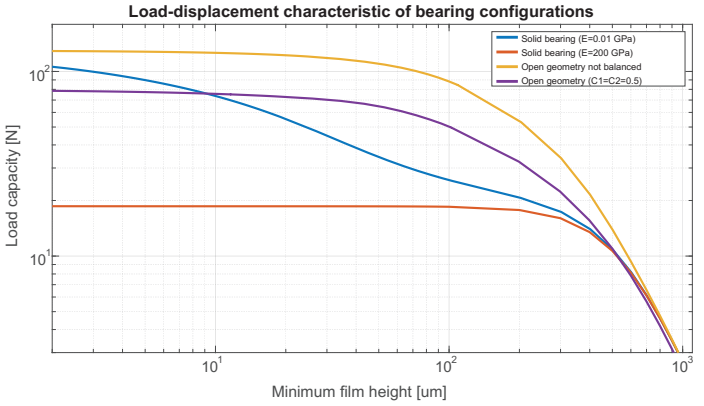

Fig. 9. Load-displacement chracteristics of all configurations. The pressure balanced configuration causes at lower film height to become more parallel then the solid rubber bearing.

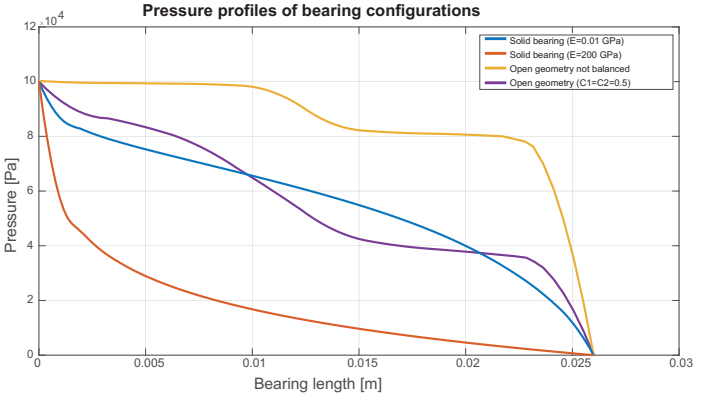

Fig. 10. Pressure profiles of all configurations at a film height of 2 μm. The general monotonically decreasing pressure in both open form geometries is concurrent with the virtual recess chambers that are created by the film pressure.

the 2 % contact surface constraint is reached. The final film height configurations and corresponding values of A_c can be seen in figure 11. With curvature, $C_1 = C_2 = 0.7$ was used in order to achieve numerical stability throughout convergence for the pressure balanced geometry. At these configuration for the solid geometry, open geometry and the open geometry with pressure balancing the stress ratios are $\lambda_{\text{stress}} = 142$, $\lambda_{\text{stress}} = 8.26$ and $\lambda_{\text{stress}} = 57.1$ respectively. The pressure balanced geometry is unable to achieve the same amount of deformation as its non-balanced counterpart, but the general trend of lower stress levels remains.

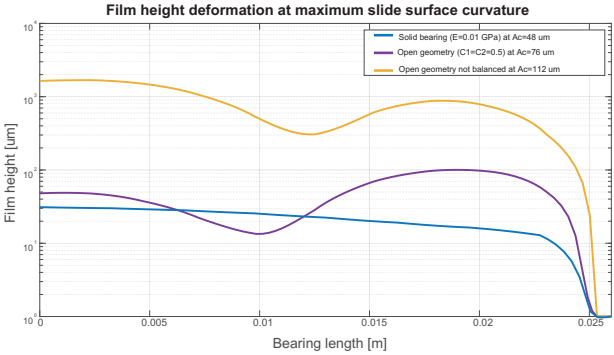

Fig. 11. Film height of the final configurations at different curvature values A_c presented with a semi-log scale. All have obtained 2 % contact at the edge.

4 Conclusion

Pressure balancing has been implemented in a basic geometry to show its potential. By tuning the chamber pressure by connecting it to the film pressure a balancing effect can be obtained that in this work is used to approximate high stiffness zero recess bearing geometry performance. In all cases with this basic open geometry seen in figure 4 a trade-off is usually made between the stiffness properties of the solid geometry and the deformation capabilities of the open geometry. The general trend however is that lower stress levels can be obtained by pressure balancing. The deformation capabilities have only been analyzed on a very basic level but show potential, especially in terms of stress factor that is favorable for the pressure balanced geometry. Future work will further investigate the fundamentals of the principle as well as different design geometries.

References

1. van Beek, A., Segal A.: Rubber Supported Hydrostatic thrust bearings with rigid bearing surfaces, Tribol. Inter., 1997, Vol. 30, pp. 47-52.
2. van Beek A., Lepic L.: Rubber Supported Hydrostatic thrust bearings with elastic bearing surfaces of infinite length, Wear, 1996, Wear 204, pp. 45-50.
3. van Ostayen, R.A.J.: The hydro-support, an elasto-hydrostatic thrust bearing with mixed lubrication, Dissertation, Delft University of Technology, 2002.
4. Herder J.L.: Energy free systems, Dissertation, Delft University of Technology.
5. Cohen T., Kurzeja P., Bertoldi K.: Architected squirt-flow materials for energy dissipation, Journal of the Mechanics and Physics of Solids, 2017, Vol. 109, pp. 22-33.
6. Bassani R., Piccigallo B., Hydrostatic Lubrication, Elsevier, 1992.